Available online at www.sciencedirect.com
ScienceDirect
Journal of the European Ceramic Society 26 (2006) 3253–3264
www.elsevier.com/locate/jeurceramsoc

Interaction between metallic interconnect and constituent oxides of (La, Sr)MnO_3 coating of solid oxide fuel cells

Y.D. Zhen, San Ping Jiang *, Sam Zhang, Vincent Tan

School of Mechanical and Aerospace Engineering, Nanyang Technological University, 50 Nanyang Avenue, Singapore 639798, Singapore

Received 7 July 2005; received in revised form 23 September 2005; accepted 8 October 2005
Available online 10 November 2005

Abstract

The chemical interaction between Fe–Cr alloy interconnect and constituent oxides of Sr-doped $LaMnO_3$ (LSM) coating, La_2O_3, SrO and Mn_2O_3, is investigated at 800–900 °C in air. The Cr deposition reaction between the Fe–Cr alloy metallic interconnect and oxides varies significantly with the nature of the oxides. The interaction between the Fe–Cr alloy and La_2O_3 and Mn_2O_3 oxide coatings primarily results in the formation of $LaCrO_3$ and $(Cr, Mn)_3O_4$ while in the case of SrO oxide coating, Cr_2O_3 is the main product. In the case of LSM coating, the formation of $(Cr, Mn)_3O_4$ and Cr_2O_3 is identified. The results indicate that the chemical interaction between the Fe–Cr alloy interconnect and LSM coating is most likely related to the surface oxide species such as SrO and MnO_x initially enriched or segregated on the surface of LSM particularly in the early stages of the reaction.

Keywords: Interface; Chemical properties; Perovskite; Fuel cells; Metallic interconnect; (La, Sr)MnO_3

1. Introduction

The reduction of the operation temperature of solid oxide fuel cells (SOFC) from 1000 °C to 600–800 °C can significantly increase materials stability and widen the material selection for fuel cell components. In particular, a lower operation temperature makes it possible to use metallic interconnect to replace the ceramic interconnect for planar-type SOFC. Metallic materials have many advantages compared with the $LaCrO_3$-based ceramic interconnect materials, which include higher thermal and electronic conductivities, good mechanical strength, ease of fabrication and significantly lower cost.[1]

Several kinds of high-temperature alloys such as Fe-based alloy,[2,3] Cr-based heat resistance alloy[4] and chromia-forming alloys[5] have been studied as the metallic interconnect. In general, these candidate alloys contain chromium as alloying element since they form an electronically conductive oxide scale on the surface by preferential oxidation of chromium to chromia (Cr_2O_3) in air as well as in fuel atmospheres.[6,7] The oxide scale prevents further oxidation of the metallic interconnect. However, at high temperatures chromium oxide generates volatile high-valent Cr-containing species in oxidizing atmospheres.[8] Without effective protective coating, the volatile Cr species causes rapid degradation of the SOFC performance due to the chemical interaction of Cr species at the (La, Sr)MnO_3 (LSM) electrode.[9–11] Thus, it is important to reduce and to inhibit the evaporation of Cr species. One approach is to add some rare earth elements, such as Y, Zr, La and Ce, into the alloy to reduce to oxide scale growth rate as well as to increase the electric conductivity of the oxide scale[12]; the other is to deposit a dense and electronic conducting coating onto the surface of the alloy to decrease the oxidation rate of the alloy and to reduce the Cr vaporization.[13–16]

LSM-based materials have been investigated as protective coating for chromia-forming alloy interconnect due to its high electrical conductivity and thermal compatibility and stability in oxidizing environment.[13–15] LSM is also a well known cathode material for SOFC.[17] Quadakkers et al.[13] studied the chemical interaction between chromia-forming alloys and oxide coatings of LSM, $LaCoO_3$ and Sr-doped $LaCoO_3$ (LSC). After heating at 950 °C for 500 h, there was significant interaction between the alloy and the oxide coatings. In the case of LSM coating, the deposition of Cr species was over the whole width of the coating, forming $MnCr_2O_4$ spinel particularly at the outer layer of the coating. Sr enrichment was observed at the interface between

* Corresponding author. Tel.: +65 6790 5010; fax: +65 6791 1859.
E-mail address: mspjiang@ntu.edu.sg (S.P. Jiang).

0955-2219/$ – see front matter © 2005 Elsevier Ltd. All rights reserved.
doi:10.1016/j.jeurceramsoc.2005.10.002

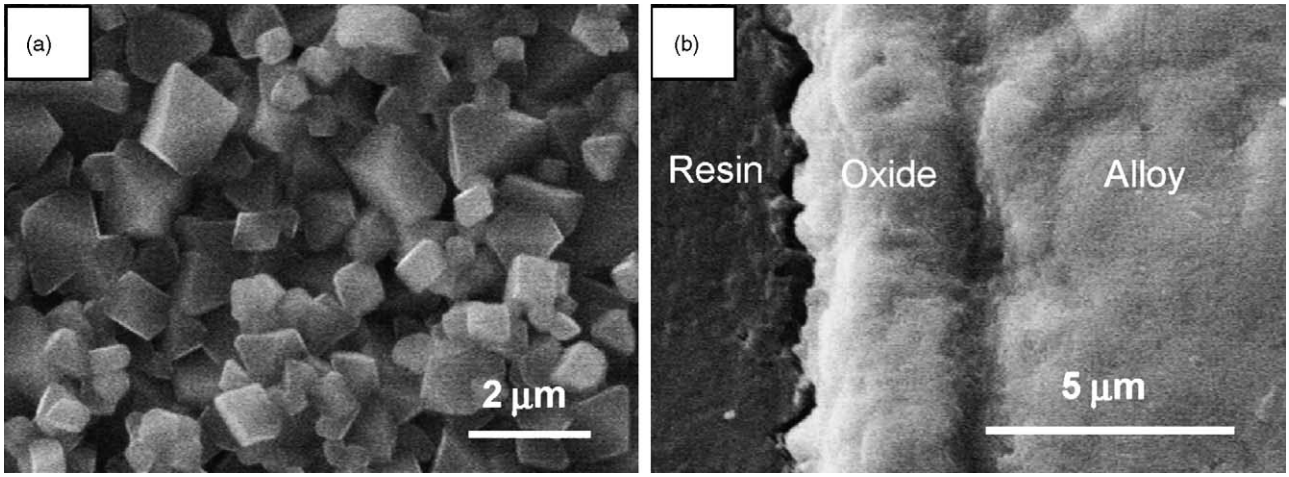

Fig. 1. SEM micrographs of the (a) surface and (b) cross-section of Fe–Cr alloy after the oxidation in air at 900 °C for 100 h.

the alloy and LSM coating. In the case of LSC coating, the Sr enrichment at the alloy/LSC interface was far more pronounced than that observed for the LSM coating. Li and Xiao[15] studied the interface between the $La_{0.8}Sr_{0.2}MnO_3$ coating and a chromia-forming alloy (Cr–5Fe–1Y_2O_3) and only found the formation of $(Mn, Cr)_3O_4$ spinel at the interface.

In the case of LSM materials, the surface composition may not be the same as that in the bulk.[18] It is also a common practice to use A-site non-stoichiometric LSM to inhibit the interface reaction between LSM and YSZ electrolyte and to enhance the stability of the LSM electrodes.[19,20] Thus, the excess or segregation of oxide species on the LSM-based protective oxide coatings could have significant effect on the chemical interaction between the Fe–Cr alloy metallic interconnect and the oxide coating. In this paper, the chemical reaction between a Fe–Cr alloy and the constituent oxides of the LSM was investigated at 800–900 °C in air. The results indicate that the chemical interaction between LSM coating and Fe–Cr alloy interconnect is in nature related to the oxide species enriched at the LSM surface, especially in the early stage of the reaction.

2. Experimental

A commercial Fe–Cr alloy, RA446 (Rolled Alloy Co., USA), was selected as the metallic interconnect material in this study and the alloy contains 24% Cr, 1.5% Mn, 1% Si, 0.2% C, 0.12% N with Fe as remaining. The alloys were cut to rectangular shape with dimension of 20 mm × 10 mm × 7 mm (width × length × height) and were ground with SiC paper of 180–1000 grit. After being polished with 3 μm diamond paste, the samples were ultrasonically cleaned in distilled water and acetone.

The constitute oxides of the LSM electrode, La_2O_3, SrO and Mn_2O_3, were investigated in this study. La_2O_3 (PIKEM Ltd., 99.9%) was pre-calcined at 1000 °C for 6 h to prevent the formation of $La(OH)_3$ phase. SrO and Mn_2O_3 powders were prepared by the decomposition of $SrCO_3$ (Merck, 99%) and $MnCO_3$ (Merck, 99%) at 1150 °C and 950 °C, respectively. LSM powder with A-site non-stoichiometric composition, $(La_{0.80}Sr_{0.20})_{0.90}MnO_3$, was synthesized by solid-state reaction process. The required amount of La_2O_3, $SrCO_3$ and $MnCO_3$ powders were mixed for 20 h using ballmilling and were calcined at 900 °C for 30 h. The phases of the respective oxides and LSM powder were confirmed by XRD analysis.

The oxide paste was prepared by mixing the oxide powder and 5 wt.% polyethylene glycol in a mortar with a pestle. The oxide coatings were deposited on the polished surfaces of alloy substrate by screen-printing. The thickness of the coatings was about 30–50 μm. All oxide-coated alloy samples were heated in open air at 900 °C and/or 800 °C for up to 500 h. The oxidation behavior of un-coated Cr alloy was also studied at 900 °C in air. The thermal expansion coefficient of the

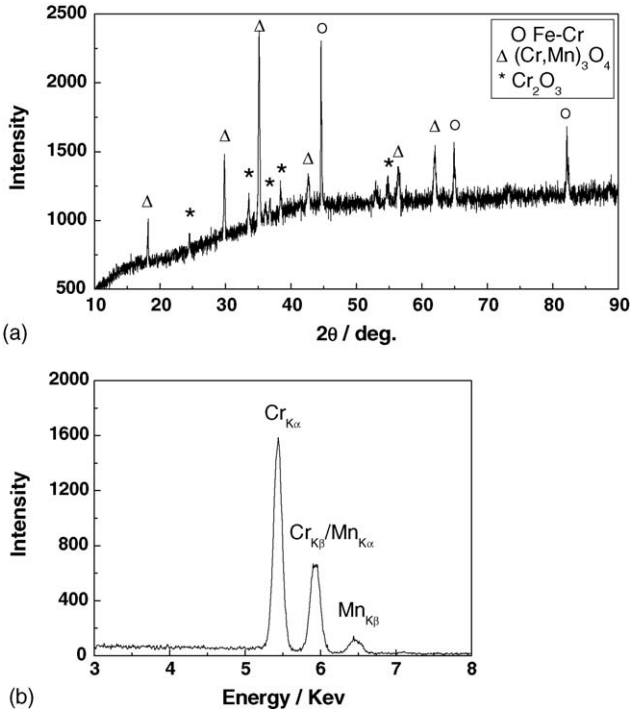

Fig. 2. (a) XRD patterns of the oxide scale surface and (b) EDS patterns of the crystals of the Fe–Cr alloy surface after oxidation at 900 °C for 100 h.

RA446 alloy was determined from room temperature to 900 °C in flowing N_2 atmosphere by a Perkin-Elemer Series 7 thermal analysis system. The thermal expansion coefficient of the alloy was 12.5×10^{-6} mm K^{-1}, which is slightly higher than that of the LSM electrode and YSZ electrolyte materials used in SOFC.[21]

The phase composition of the samples after oxidation was identified by XRD (Philips PW 1830). The morphology and microstructure of the surface as well as the cross-section of the samples were examined by scanning electron microscopy (SEM, Leica 360). Au was sputtered to the SEM specimen to improve the conductivity. Distribution profile of the elements was examined by the energy dispersive X-ray analysis system (EDS, Oxford) using linear scanning mode.

To study the gas-phase transportation of Cr species, La_2O_3 and SrO oxides were pressed into small disks with a diameter of 8 mm and thickness of about 3 mm. The oxide disks were arranged about 5 mm away from the Fe–Cr alloy and there was no direct contact between the disk and the alloy. Both the oxide disk and alloy samples were placed inside a crucible. Oxidation treatments were also carried out in open air at 900 °C for 500 h. The deposition of Cr species was indicated by the color change of the oxide samples.

3. Results and discussion

3.1. Oxidation of Fe–Cr alloy

Fig. 1 shows the SEM micrographs of the surface and cross-section of a Fe–Cr alloy after the oxidation in air at 900 °C for 100 h. A thick and dense oxide scale layer was formed on the alloy surface (Fig. 1b). The oxide scale was continuous and the average thickness was 3 μm. The oxide scale at the alloy interface was dense without any voids and cracks, indicating the good adhesion of the oxide scale to the alloy substrate. The morphology of the oxide scale surface was characterized by the dense packed well-faceted crystal (Fig. 1a).

Fig. 2 shows the XRD and EDS patterns of the oxide scale. From XRD analysis, the identified phases on the oxidized alloy surface were (Cr, $Mn)_3O_4$-type spinel oxide, Cr_2O_3 oxide as well as the Fe of the original alloy (Fig. 2a). EDS analysis of the crystals shows the existence of Cr and Mn, indicating that the well-faceted crystals were most likely (Cr, $Mn)_3O_4$ spinel. Similar phases were also observed on the surface of other Mn-containing Fe–Cr alloys, such as SUS430[3] and ZMG232.[6] The precipitation of the (Cr, $Mn)_3O_4$ spinel on the top of the chromia scale can be attributed to the high diffusion coefficients of man-

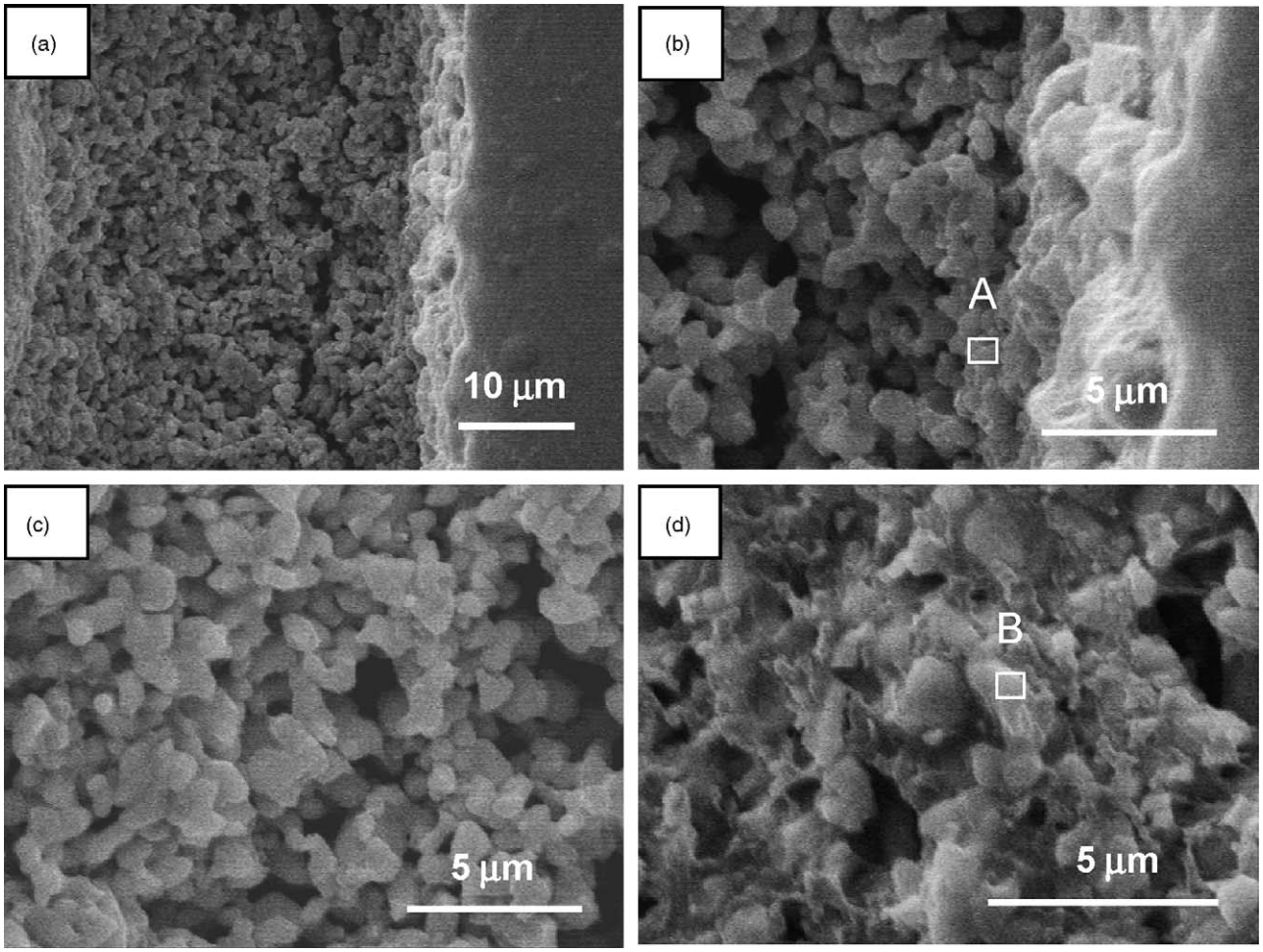

Fig. 3. SEM micrographs of the La_2O_3 coating and Fe–Cr alloy interface after oxidation treatment at 900 °C for 100 h. (a) An overview of the cross-section; (b) the Fe–Cr alloy/La_2O_3 interface; (c) the bulk region of the coating; and (d) the region close to the surface of the coating.

ganese ions. The metal ion diffusion decreases in the order of $D_{Mn} > D_{Fe} > D_{Cr}$ by assuming that these metal ions diffuse via Cr^{3+}-lattice sites in Cr_2O_3.[22] Based on the Cr–Mn–O system phase diagram the $(Cr, Mn)_3O_4$ spinel is thermodynamically favorable even at low Mn concentration.[23] The formation of the $(Cr, Mn)_3O_4$ spinel layer on the oxide scale could reduce significantly the vaporization pressure of gaseous chromium species.

3.2. La_2O_3-coated Fe–Cr alloy

The La_2O_3 coating was originally white in color before the oxidation experiment. After oxidation in air at 900 °C for 100 h, the color of the coating changed to brownish yellow, indicating the interaction between the Fe–Cr alloy and the La_2O_3 coating. Fig. 3 shows the SEM micrographs of the La_2O_3 coating and Fe–Cr alloy interface after oxidation at 900 °C for 100 h and Fig. 4 is the corresponding element distribution profile and EDS patterns taken at different regions of the oxide coating. The oxide scale was ~2–4 μm thick and was not uniform in comparison to that of un-coated alloy (Fig. 3a and b). There was a significant increase in the Mn content in the oxide scale towards the interface between the alloy and the La_2O_3 oxide coating (Fig. 4a). This probably indicates the formation of $(Cr, Mn)_3O_4$ spinel phase on the surface of the oxide scale, consistent with that observed on the un-coated Fe–Cr alloy (Fig. 1).

The La_2O_3 coating was porous and the morphology of the coating in the region close to the alloy interface was characterized by the sphere-shaped particles of about 0.5 μm. The bonding between the La_2O_3 oxide coating and the Fe–Cr alloy appears to be good (Fig. 3b). In the region close to the air side of the coating, there were flake-like particles in the coating (Fig. 3d). This may be due to the formation of lanthanum hydroxide as the La_2O_3 is easy to absorb moisture when exposed in air. The elemental distribution analysis shows that Cr was present over the whole La_2O_3, indicating that the Cr deposition occurred over the whole oxide coating (Fig. 4a). Moreover, the profile of Cr followed closely with that of La and the atomic ratio of Cr/La was almost equal to one, probably indicating the formation of the $LaCrO_3$ phase. The close profile of La and Cr in the oxide coating also indicates that La_2O_3 can readily react with Cr species. In the areas close to the alloy interface, there was a significant deposition of Cr. This is indicated by the much smaller $La_{L\alpha}/La_{L\beta}$ ratio of 0.62 taken at the La_2O_3 coating region of ~2 μm from the alloy interface (Fig. 4b), as compared to the ratio of 4.81 for the pure La_2O_3 oxide (Fig. 4d). The reduction in the $La_{L\alpha}/La_{L\beta}$ ratio is due to the fact that the Kα X-ray

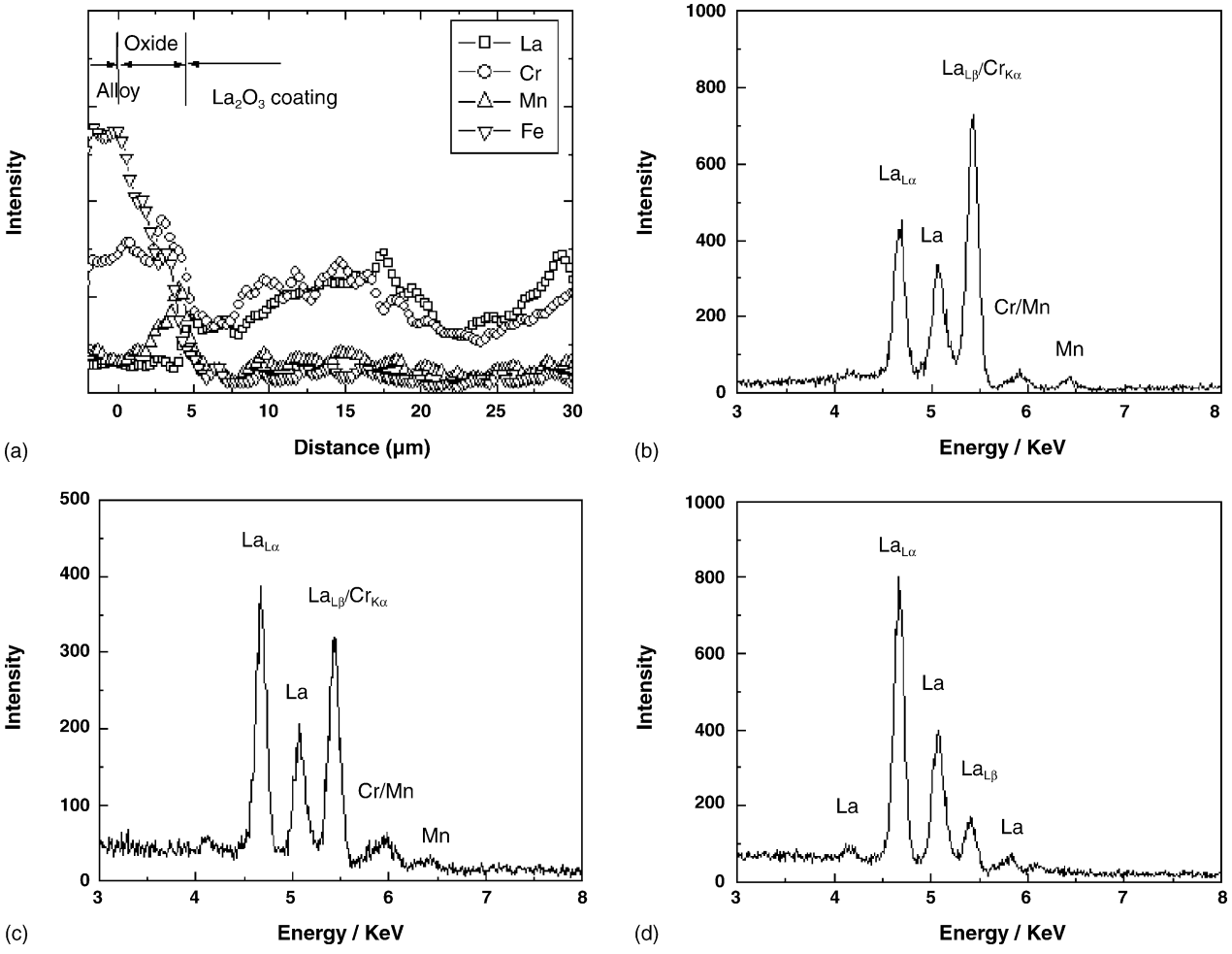

Fig. 4. (a) Element distribution profile of La_2O_3 oxide coating and EDS patterns taken at (b) 2 μm (point A in Fig. 3b) from the interface and (c) 10 μm (point B in Fig. 3d) from the interface. The EDS pattern of pure La_2O_3 oxide is shown in (d).

peak of Cr is overlapped with the Lβ peak for La. As the coating distance increased to 10 μm from the oxide coating/alloy interface, the $La_{L\alpha}/La_{L\beta}$ ratio increased to 1.24 (Fig. 4c). The higher $La_{L\alpha}/La_{L\beta}$ ratio as compared to that measured at the area close to the interface (Fig. 4b) indicated the decrease in the Cr deposition.

It is noted the presence of the Mn from the EDS analysis of the La_2O_3 oxide coating and the intensity of the Mn is more or less the same cross the whole La_2O_3 coating (Fig. 4b and c). This indicates that Mn diffused from the oxide scale of the alloy into the oxide coating. This seems to indicate that manganese species are mobile, consistent with that observed for the LSM cathodes under cathodic polarization conditions.[10,11] On the other hand, Fe peak at 7.2 keV was barely visible, indicating that the Fe signal in the element distribution profile could be the background noise (Fig. 4a).

3.3. SrO-coated Fe–Cr alloy

SrO coating deposited on the Fe–Cr alloy had poor adhesion and the coating was completely peeled off from the surface of alloy after the oxidation experiments at 900 °C. However, the SrO coating deposited on the Fe–Cr alloy oxidized in air at 800 °C for 100 h was survived. After the oxidation treatment, the SrO coating changed from the original white color to the green, indicating the deposition Cr species in the SrO coating. Fig. 5 shows the SEM micrographs of the cross-section of the SrO coating/Fe–Cr alloy after oxidation treatment in air at 800 °C for 100 h and Fig. 6 is the corresponding element distribution profile and EDS analysis of selected regions. There was a gap formed between the SrO coating and the alloy, indicating the poor adhesion. The SrO coating was characterized by the significant formation of plate-like particles. EDS analysis of the plate-like particles shows the significant presence of Cr (Fig. 6b) while in the areas with no plate-like particles, the Cr content was very small (Fig. 6c). This shows that Cr deposition in the SrO coating is not uniform, which is consistent with the element distribution profile of the SrO coating (Fig. 6a). The plate-like particles are most likely Cr_2O_3 phases and this is also supported by the observation of the green color of the coating after the oxidation at 800 °C. Cr_2O_3 is a well-known green pigment.[24] On the other hand, the formation of $SrCrO_4$ would give distinguish strontium yellow.[24] Very different from that in the case of the La_2O_3 coating (Fig. 4a), the distribution of Cr did not

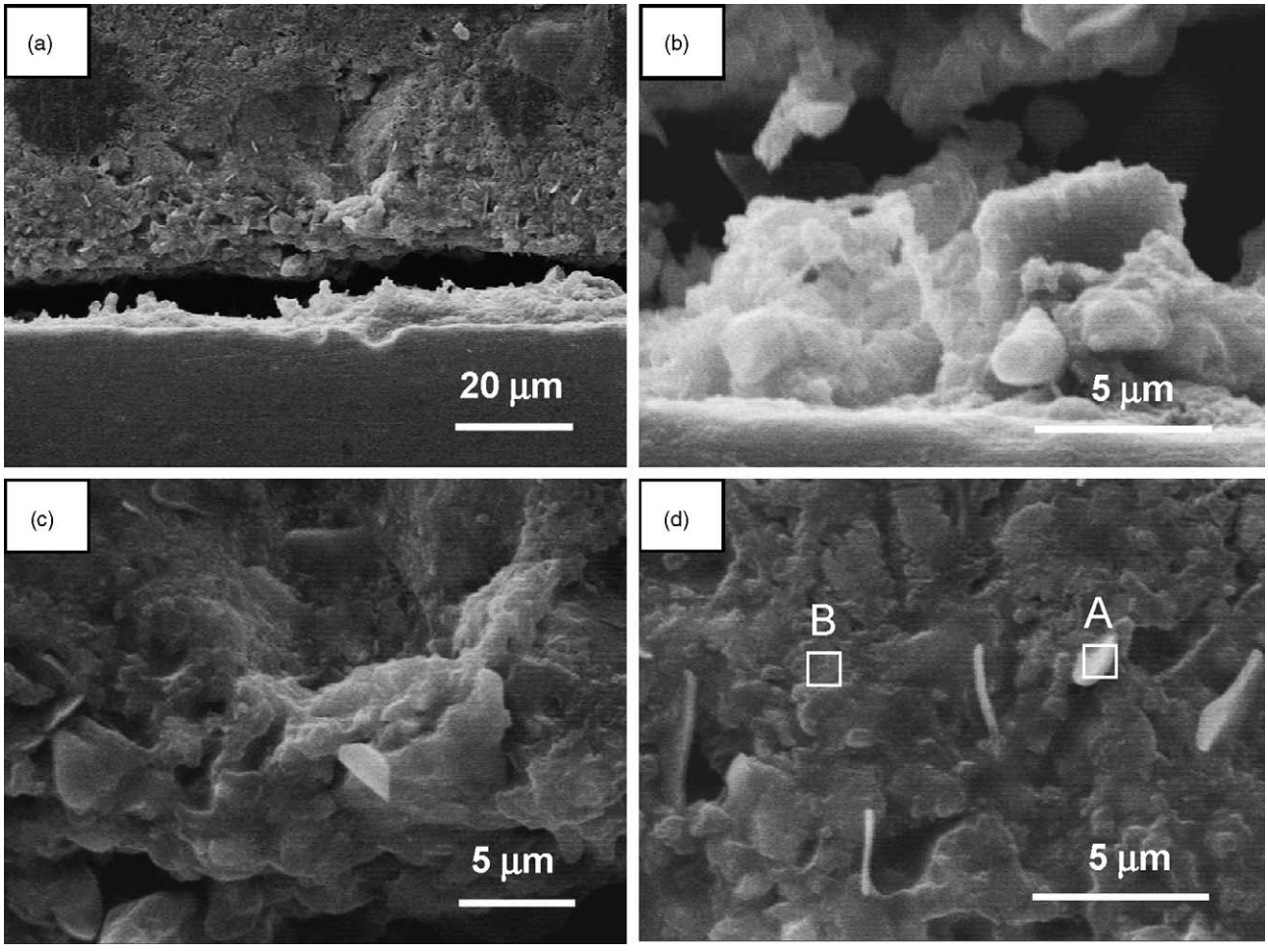

Fig. 5. SEM micrographs of the SrO coating/Fe–Cr alloy after oxidation treatment in air at 800 °C for 100 h. (a) An overview of the cross-section; (b) the Fe–Cr alloy/SrO interface; (c) the bulk region of the coating; and (d) the region close to the air side of the coating.

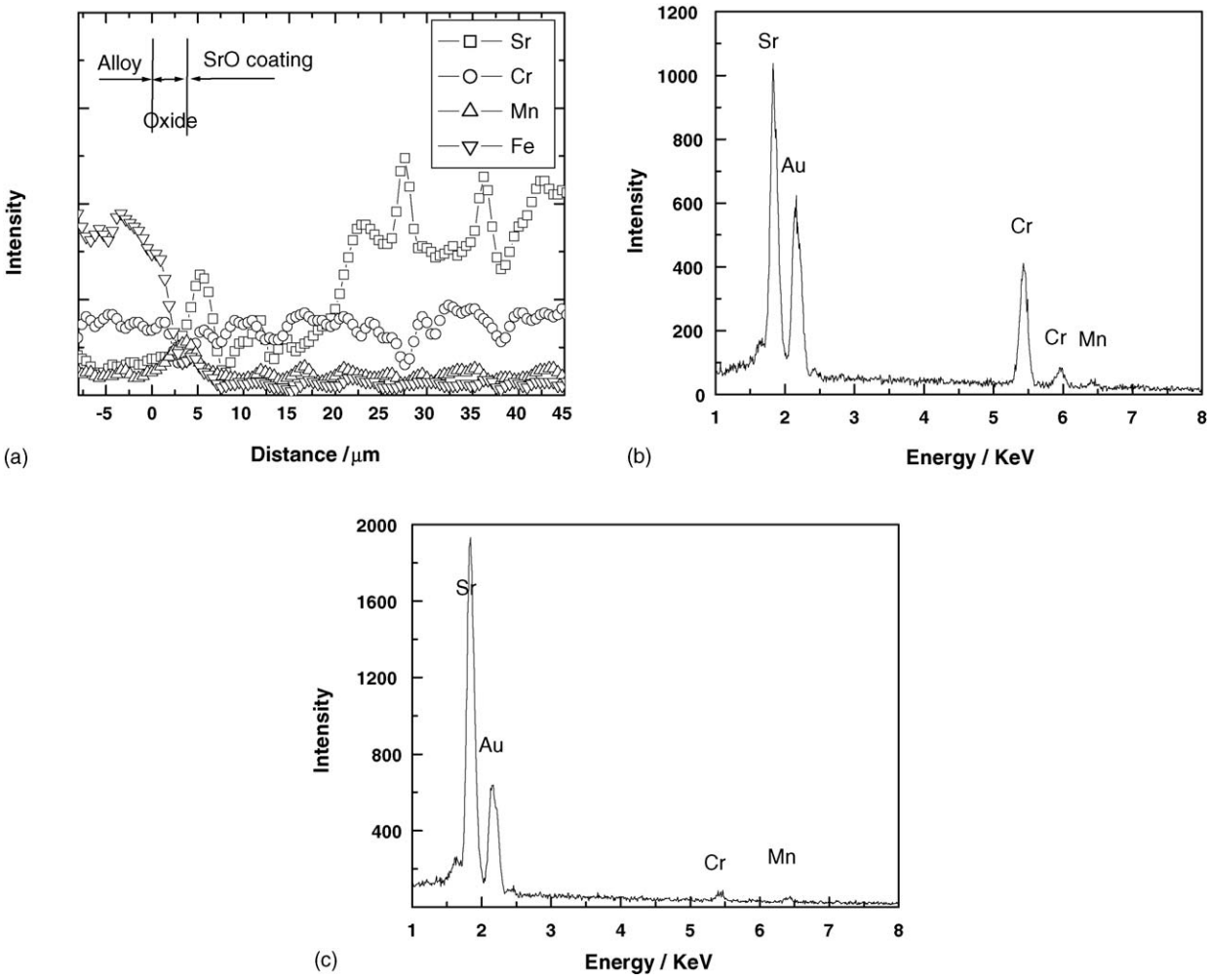

Fig. 6. (a) Element distribution profile of the SrO oxide coating and EDS analysis of (b) the plate-like particles (point A in Fig. 5d) and (c) the areas with no plate-like particles (point B in Fig. 5d).

follow that of Sr and the atomic ratio of Cr/Sr was far below one. The mismatch of the Cr and Sr element distribution profile and the formation of plate-like particles indicate that the interaction between the SrO and Fe–Cr alloy primarily lead to the deposition of Cr_2O_3 rather than the formation of $SrCrO_4$. The diffusion of Mn from the oxide scale into SrO coating was also evident (Fig. 6b and c), consistent with that observed for the La_2O_3 oxide coating. The Au signal in the EDS pattern was due to the sputtered Au in order to improve the conductivity of the SEM specimen.

3.4. Mn_2O_3-coated Fe–Cr alloy

Fig. 7 shows the SEM micrograph of the cross-section of the Mn_2O_3 coating/Fe–Cr alloy interface after the oxidation treatment in air at 900 °C for 500 h and Fig. 8 is the corresponding element distribution profile and the EDS analysis of selected regions. The thickness of oxide scale was about 5 μm. The morphology of the coating was characterized by fine grains and some large particles (Fig. 7b). EDS analysis showed that the fine particles contained significant amount of Mn as compared to Cr with Cr/Mn ratio of ∼0.31 (Fig. 8b) and on the other hand the large particles contained much higher Cr and the Cr/Mn ratio was ∼0.78 (Fig. 8c). This indicates that the large particles in the Mn_2O_3 coating may be the $(Cr, Mn)_3O_4$ spinel phase with high Cr content. The distribution profile of Cr in the Mn_2O_3 coating generally followed that of Mn, similar to that of the La_2O_3 oxide coating. As shown in the case of SrO oxide coating, the formation of Cr_2O_3 phase would result in the non-uniform distribution of Cr in the oxide coating (Fig. 6a). However, the atomic ratio of Cr/Mn was less than one and varied somehow within the Mn_2O_3 coating. This indicates that the product of the Cr deposition in the Mn_2O_3 oxide coating would be primarily $(Cr, Mn)_3O_4$ phase with Cr/Mn ratio less than one. Thus, Mn_2O_3 would facilitate the deposition of Cr species, leading to the preferential formation of the $(Cr, Mn)_3O_4$ spinel phase.

3.5. LSM-coated Fe–Cr alloy

Fig. 9 shows the SEM micrographs of the cross-section of the interface between the LSM coating and Fe–Cr alloy after oxidation in air at 900 °C for 100 h. Fig. 10 is the EDS patterns of the selected regions of the LSM coating. The formation of an oxide scale layer at the alloy/LSM coating interface can be clearly seen.

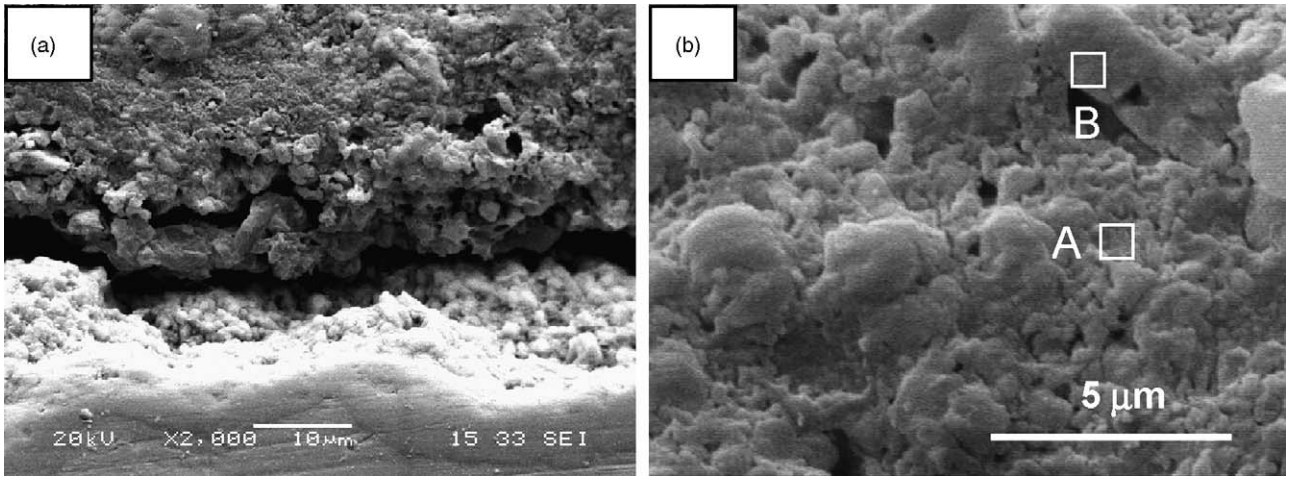

Fig. 7. SEM micrograph of the Mn_2O_3 coating/Fe–Cr alloy interface after oxidation treatment in air at 900 °C for 500 h. (a) The overview of the cross-section and (b) the bulk region of the coating.

The oxide scale contains the Cr, Mn and Fe, similar to that on the un-coated alloy (Fig. 10a). However, the oxide scale formed was much thinner and not uniform on the LSM-coated Fe–Cr alloy compared with the un-coated alloy, indicating that LSM coating affects the oxidation behavior of the Fe–Cr alloy. The screen-printed LSM coating is porous and the contact between the LSM coating and Fe–Cr alloy appears to be good (Fig. 9b). Throughout the whole coating region, the morphology of the

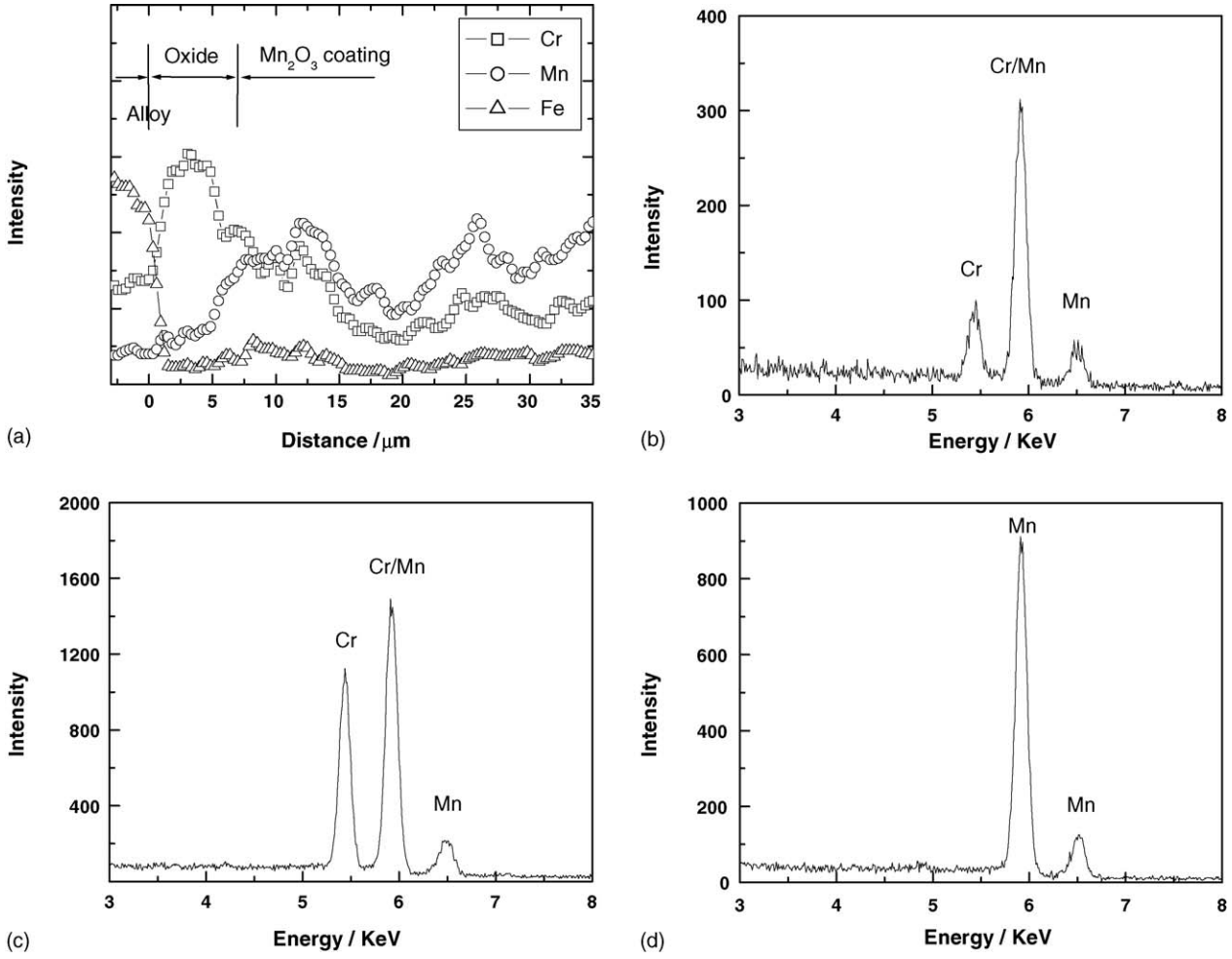

Fig. 8. (a) Element distribution profile of the Mn_2O_3 oxide coating and EDS analysis of (b) region with small grains (point A in Fig. 7b) and (c) region with particle (point B in Fig. 7b). The EDS pattern of pure Mn_2O_3 is shown in (d).

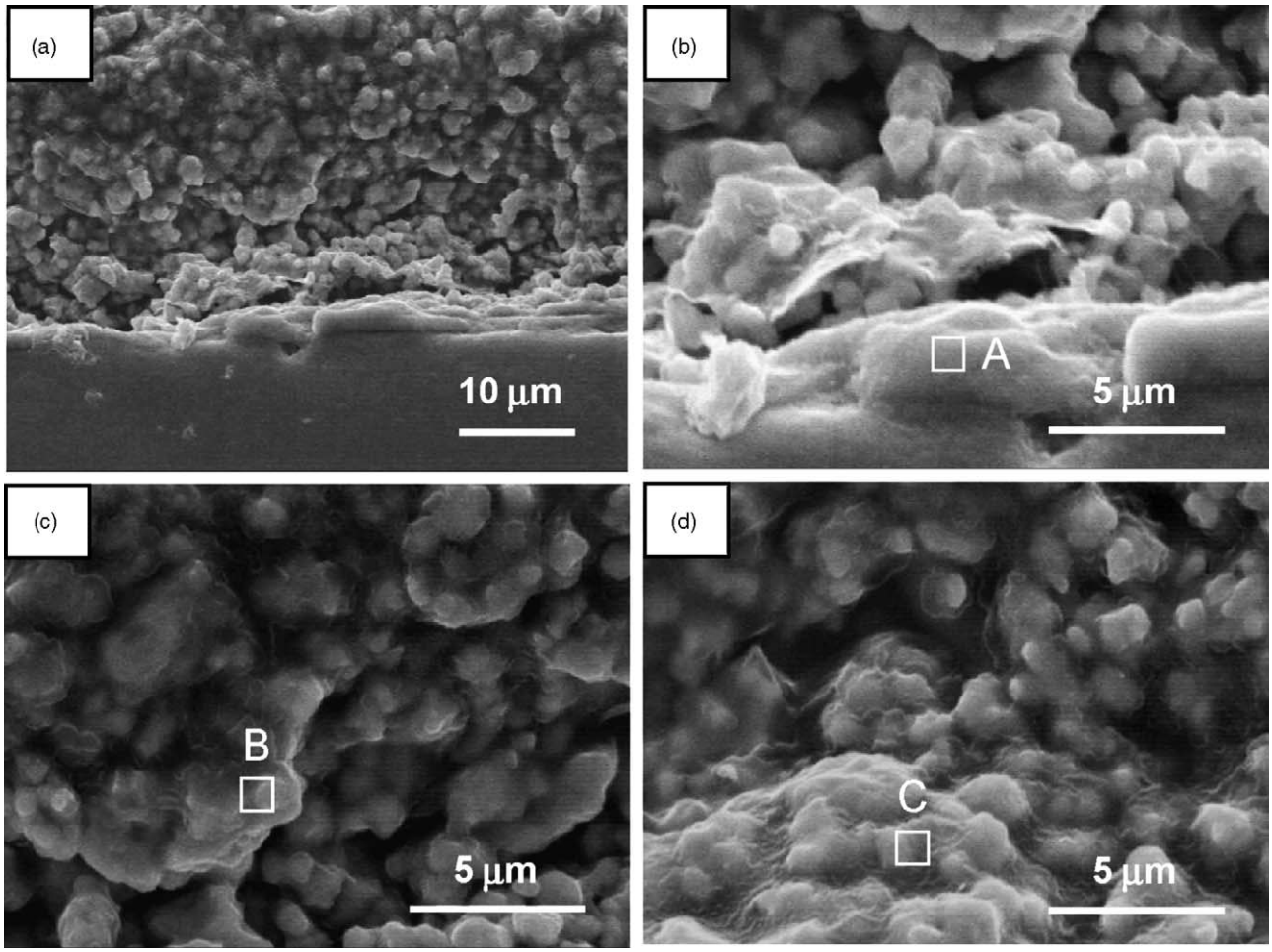

Fig. 9. SEM micrographs of the cross-section of the interface between the LSM coating and Fe–Cr alloy after oxidation at 900 °C for 100 h. (a) An overview of the cross-section; (b) the Fe–Cr alloy/LSM interface; (c) the coating bulk region; and (d) the top surface of the LSM coating.

LSM coating was quite uniform and the LSM grain size was ~1 μm (Fig. 9). However, the deposition and distribution of Cr species varied with the thickness of LSM coating. It is known that on the EDS patterns the Kα X-ray peak of Cr is overlapped with the Lβ peak for La meanwhile the Kα peak of Mn overlaps with the Kβ peak for Cr. Nevertheless, the presence of Cr can be verified from the variation in the intensity ratio of Lα/Lβ for La in LSM/alloy couple as compared to that of pure LSM. For pure LSM, the $La_{L\alpha}/La_{L\beta}$ ratio was 4.38 (Fig. 10d). The $La_{L\alpha}/La_{L\beta}$ ratio of the LSM coating/Fe–Cr alloy was 2.21 and 2.98 in the LSM coating region at a distance of 5 and 10 μm away from the LSM/alloy interface (Fig. 10b and c). The lower $La_{L\alpha}/La_{L\beta}$ ratio indicates the higher content of Cr in the coating. This indicates that Cr deposition in the LSM coating decreases with the distance away from the alloy surface.

Fig. 11 shows the SEM micrograph and the element distribution profile of the LSM coating/Fe–Cr alloy interface after oxidation at 900 °C for 500 h. A gap between the LSM coating and Fe–Cr alloy substrate was observed, which could be formed during the cooling of the sample or during the SEM specimen preparation. In areas close to the alloy/LSM interface, the microstructure of the LSM coating is characterized by fine grains, similar to that oxidized for 100 h under the same temperature (Fig. 9). In the areas 20 μm away from the LSM coating/Fe–Cr alloy interface, there was formation of plate-like particles (Fig. 11a). The size of the plate-like particles varies and the morphology of the plate-like particles is similar to that observed for the SrO/Fe–Cr alloy couple (Fig. 5). EDS analysis revealed that these particles contain chromium as the intensity ratio of $La_{L\alpha}/La_{L\beta}$ was 2.69 (Fig. 11d), which is significantly lower than 4.38 of the pure LSM particle. The formation of plate-like particles probably indicates the formation of Cr_2O_3 phase in addition to the formation of $(Cr, Mn)_3O_4$ as shown by Quadakkers et al.[13] and Li and Xiao.[15]

From the distribution profile of the elements (Fig. 11c), there was a high concentration of Mn in the oxide scale, which is consistent with the observed formation of the $(Cr, Mn)_3O_4$ spinel at the outer surface of the oxide scale (Fig. 2a). In the LSM coating, the element distribution of La, Mn and Sr is quite homogeneous and does not show visible enrichment of the constituent elements of the LSM in the coating. The distribution of chromium did not follow with particular elements over the whole width of the LSM coating. However, the distribution of the Cr indicates the almost uniform deposition of Cr across the whole LSM coating.

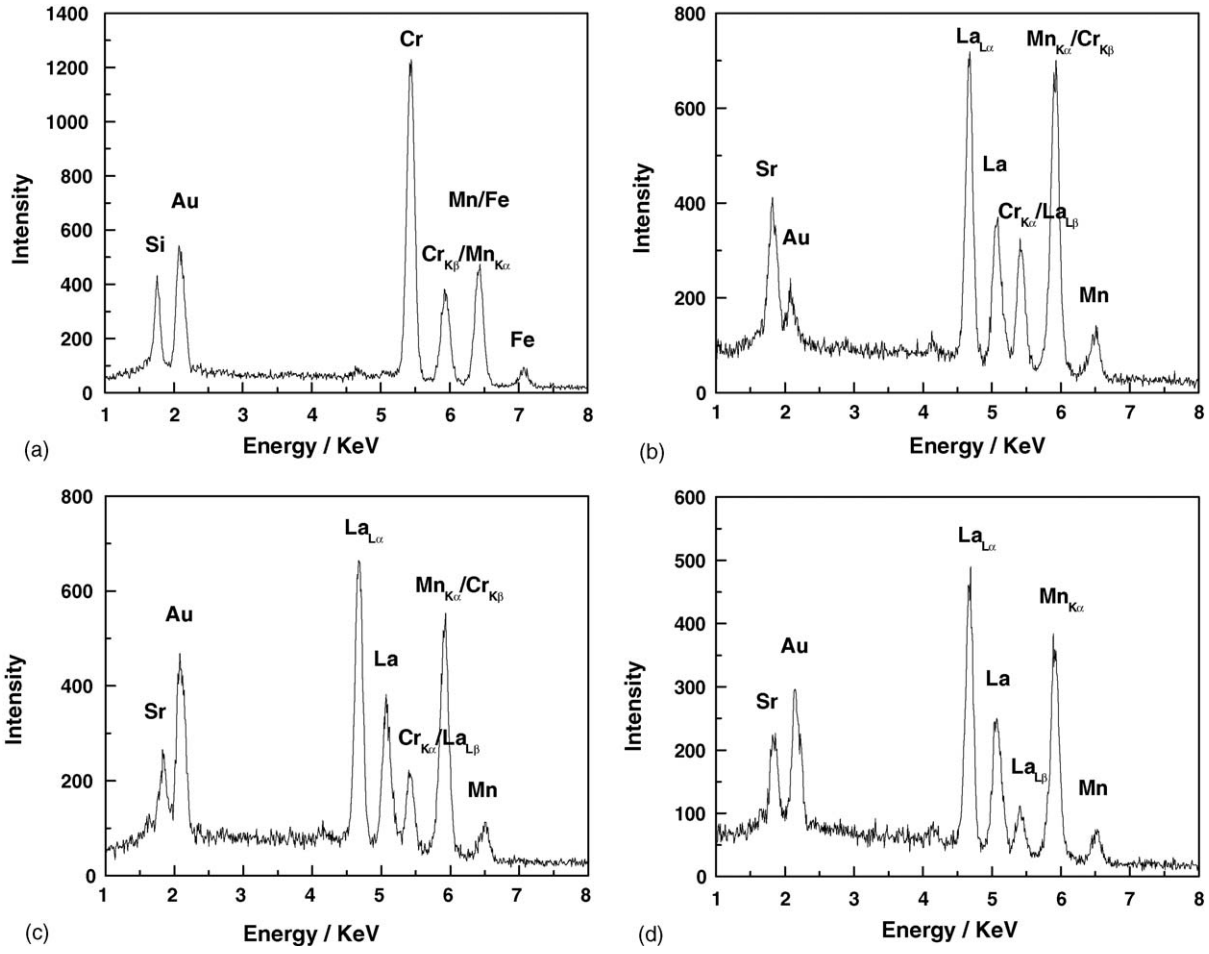

Fig. 10. EDS patterns of the selected regions of the LSM coating and Fe–Cr alloy after oxidation at 900 °C for 100 h. (a) The oxide scale (point A in Fig. 9b); (b) the bulk region of the coating (point B in Fig. 9c); and (c) the top surface of the coating (point C in Fig. 9d). The EDS pattern of pure LSM is shown in (d).

3.6. Reaction between Fe–Cr alloy and constituent oxides of LSM

Additional experiments were carried out to study the interaction between the constituent oxides (La_2O_3 and SrO) of LSM and the Fe–Cr alloy by separating the oxide disks and the alloy samples under the oxidation condition at 900 °C for 500 h. The color of La_2O_3 oxide disk changed partially from the original white to brownish yellow and in the case of the SrO oxide disk, it became green after the oxidation experiment. This is similar to that observed for the oxide coating experiments. The color change indicates again the significant deposition of Cr in the oxide disks and the transport of chromium species is most likely through the gas phase diffusion of high valent Cr species such as CrO_3 and/or $CrO_2(OH)_2$.[13]

The gaseous Cr species (e.g., CrO_3) evaporated from the oxide scale of the chromia-forming alloy can directly deposit to form Cr_2O_3 by dissociation according to the following reaction:

$$CrO_3(g) = 1/2Cr_2O_3(s) + 3/2O_2 \quad (1)$$

However, depending on the nature of the oxides, the formation of Cr_2O_3 by dissociation may not always be kinetically preferable. The results in the current study indicate that the deposition and formation of Cr compounds depend strongly on the nature of the oxide. In the cases of La_2O_3 coatings with the Fe–Cr alloy, the distribution profile of Cr closely matches that of La and the atomic ratio of Cr/La is close to unity. This shows that La has high affinities for the deposition or dissociation of Cr species. The unit atomic ratio of La/Cr probably indicates the formation of $LaCrO_3$. The formation of $LaCrO_3$ by the reaction between Cr_2O_3 and La_2O_3 is thermodynamically favorable.[25] Zhu et al.[26] deposited the La_2O_3 thin film onto a pre-oxidized stainless steel by sputtering method and observed the formation of $LaCrO_3$ phase after annealing at 800 °C for 1 h.

In the case of Mn_2O_3 oxide coating, Cr distribution also in general follows that of Mn (Fig. 8a) though the atomic ratio of Cr/Mn is less than unity. This indicates that Mn_2O_3 also has high affinities for the Cr deposition, similar to that of La_2O_3. From the Mn_2O_3–Cr_2O_3 phase diagram,[27] at high temperature (above 900 °C) Mn_2O_3 oxide would be partially reduced to Mn_3O_4 oxide, a mixture of Mn^{2+} and Mn^{3+}. Significant deposition of Cr species in the Mn_2O_3 coatings indicates the nucleation reaction

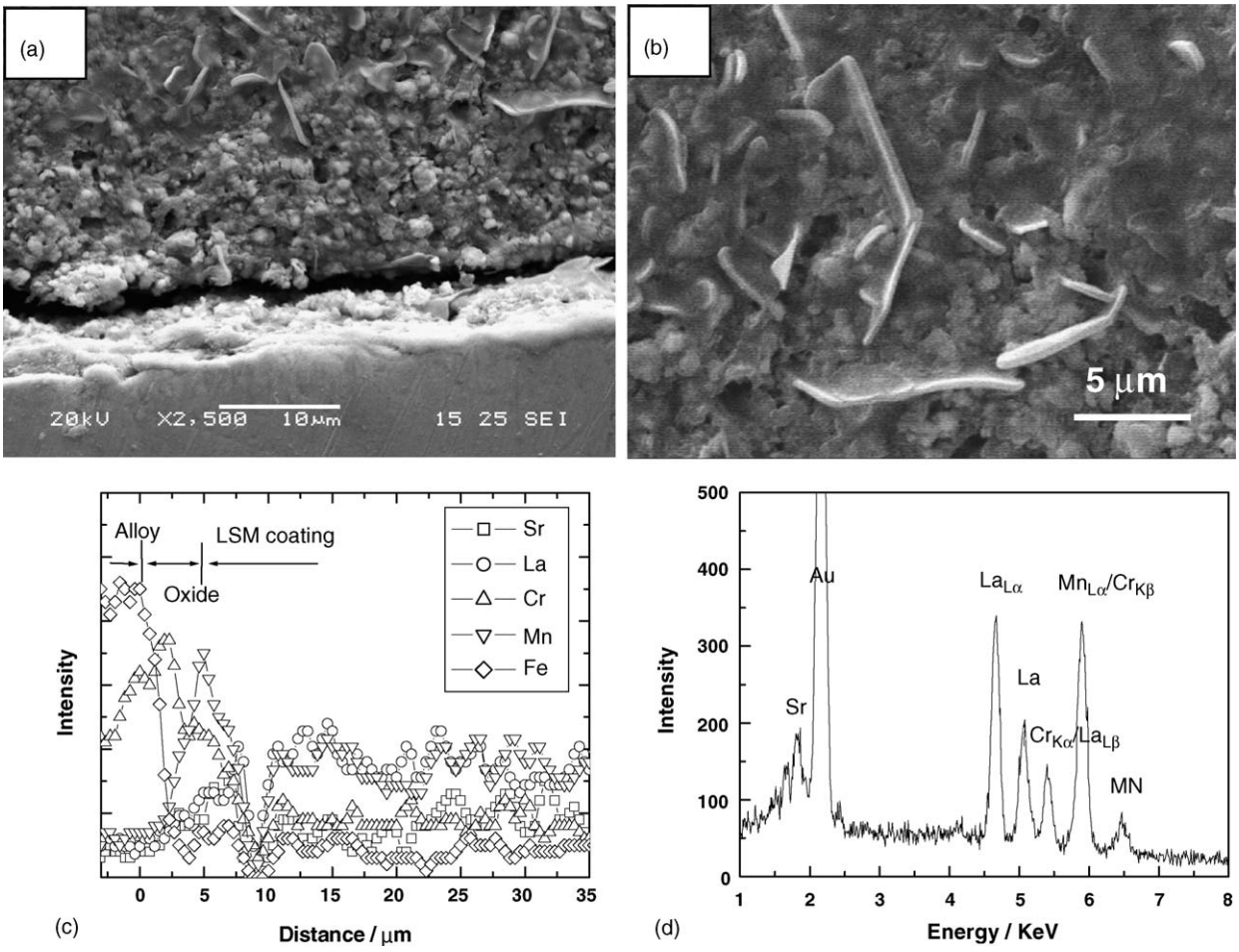

Fig. 11. SEM micrographs showing (a) the cross-section and (b) the plate-like deposits of LSM coated specimen after oxidation at 900 °C for 500 h. The element distribution profile is shown in (c) and EDS pattern of the plate-like deposit is shown in (d).

and the grain growth between the gaseous Cr species and Mn species, leading to the formation of (Cr, Mn)$_3$O$_4$ spinel phase with Cr/Mn ratio less than one under conditions of the present study.

The formation of Cr_2O_3 is most likely dominant for the chemical interaction between the SrO coating and Fe–Cr alloy. This is indicated by the appearance of green color of the original white SrO coating after the heat treatment, the very different Sr and Cr distribution profiles and the formation of the plate-like particles with high Cr content. However, the deposition of Cr_2O_3 is most likely induced by the SrO. The deposition of Cr is substantial on the LSCF electrode in the absence of polarization and this has been attributed to the originally enriched SrO species on the LSCF electrode surface.[28] Thus, the presence of SrO will lead to the preferential deposition of Cr_2O_3 phase. The formation of $SrCrO_4$ may also be possible under long-term sintering conditions. In conclusion, the main reaction between the Cr species and the constituent oxides of LSM materials at the early stage of the reaction can be written as follows.

$$CrO_3 + La_2O_3 \rightarrow LaCrO_3 + O_2 \quad (2)$$

$$CrO_3 + Mn_2O_3 \rightarrow (Cr, Mn)_3O_4 + O_2 \quad (3)$$

$$CrO_3 \xrightarrow{SrO} Cr_2O_3 + O_2 \quad (4)$$

In the case of A-site non-stoichiometric LSM electrode materials, the surface composition is not the same as that of the bulk. As shown by the acid etch analysis of the LSM electrodes prepared by chemical co-precipitation, there are Mn and Sr enrichments on the freshly prepared LSM electrode surface but not La.[29] Decorse et al.[18] investigated the surface composition of LSM and found that Sr and oxygen contents of the surface were higher than that in the bulk, indicating the segregation of SrO on the LSM surface. Viitanen et al. [30] studied the surface compositions of $La_{0.6}Sr_{0.4}Co_{0.2}Fe_{0.8}O_3$ (LSCF) oxide membranes by low-energy ion spectroscopy (LEIS). Before the oxygen permeation experiments, the LEIS measurements only showed the presence of Sr, O and some La, in the outermost atomic layer and no Fe and Co on the LSCF membranes. The segregation and enrichment of the oxides on the LSM coating surface could have significant effect on the interaction between the LSM coating and the Fe–Cr alloy. In the case of the LSM coating/Fe–Cr alloy, the formation of the (Cr, Mn)$_3$O$_4$ phase would most likely be substantial due to the significant excess of the Mn species on the LSM surface in the case of A-site non-stoichiometric LSM in the present study. This appears to be supported by the

uniform distribution of the Cr over the whole LSM coating and is in general consistent with that reported in the literature.[13] The deposition of Cr species and the formation of $(Cr, Mn)_3O_4$ spinels for the O_2 reduction on the LSM electrode in the presence of Fe–Cr alloy have been considered to be related with the Mn^{2+} species generated under cathodic polarization.[11] This is consistent with high affinities of the manganese oxides for the Cr deposition as shown in the Mn_2O_3/Fe–Cr couple (Figs. 7 and 8). The SrO species enriched/segregated on the freshly prepared LSM coating surface can lead to the preferential deposition of Cr_2O_3. This is supported by the formation of plate-like particles in both LSM/Fe–Cr alloy and SrO/Fe–Cr alloy couples. The reasons for the appearance of the plate-like particles in the LSM/Fe–Cr alloy couple after the oxidation at 900 °C for 500 h are not clear. One reason could be the increase of the Sr segregation on the LSM surface with the increase in the oxidation treatment. However, the formation of $LaCrO_3$ phase in the LSM coating/Fe–Cr alloy would be less likely under the conditions studied because there is little La segregation on the surface of the A-site non-stoichiometric LSM.[29]. Nevertheless, in the case of stoichiomtric LSM where the La enrichment can occur,[19,20] the formation of $LaCrO_3$ in the LSM coating/Fe–Cr alloy couple would be kinetically favorable, as shown by Quadakkers et al.[13]

4. Conclusions

The interaction between the constituent oxides of LSM materials such as La_2O_3, SrO and Mn_2O_3 and a Fe–Cr alloy has been investigated. In the case of La_2O_3 and Mn_2O_3 coatings, the dominant products of the reaction between the Fe–Cr alloy and the coatings are most likely $LaCrO_3$ and $(Cr, Mn)_3O_4$ while in the case of SrO, the main deposits are Cr_2O_3. The observations of the interaction between the LSM coating and Fe–Cr alloy are in general consistent with that observed between the constituent oxides of the LSM and the Fe–Cr alloy, taking into considerations of the fact that surface oxides such as SrO and MnO_x are segregated originally on the LSM surface. The results indicate that the chemical interaction between the LSM electrodes and Fe–Cr alloys would be essentially related to the nature of the oxide species segregated/enriched on the LSM coating towards deposition and reaction of gaseous Cr species.

Finally, we have observed significant Mn diffusion from the oxide scale into the oxide coating and this may have significant implications for the long-term stability and performance of the chromia-forming alloys with Mn as alloying elements.

Acknowledgement

Y.D. Zhen thanks the Nanyang Technological University for the graduate research studentship.

References

1. Fergus, J. W., Metallic interconnects for solid oxide fuel cells. *Mater. Sci. Eng. A*, 2005, **397**, 271–283.
2. Huang, K., Hou, P. Y. and Goodenough, J. B., Characterization of iron-based alloy interconnects for reduced temperature solid oxide fuel cells. *Solid State Ionics*, 2000, **129**, 237–250.
3. Brylewski, T., Nanko, M., Maruyama, T. and Przybylski, K., Application of Fe–16Cr ferritic alloy to interconnector for a solid oxide fuel cell. *Solid State Ionics*, 2001, **143**, 131–150.
4. Kadowaki, T., Shiomitsu, T., Matsuda, E., Nakagawa, H., Tsuneizumi, H. and Maruyama, T., Applicability of heat resisting alloys to the separator of planar type solid oxide fuel cell. *Solid State Ionics*, 1993, **67**, 65–69.
5. Linderoth, S., Hendriksen, P. V., Mogensen, M. and Langvad, N., Investigaiton of metallic alloys for use as interconnects in solid oxide fuel cell stacks. *J. Mater. Sci.*, 1996, **31**, 5077–5082.
6. Horita, T., Xiong, Y., Yamaji, K., Sakai, N. and Yokokawa, H., Evaluation of Fe–Cr alloys as interconnects for reduced operation temperature SOFCs. *J. Electrochem. Soc.*, 2003, **150**, A243–A248.
7. Meulenberg, W. A., Uhlenbruck, S., Wessel, E., Buchkremer, H. P. and Stöver, D., Oxidation behaviour of ferrous alloys used as interconnecting material in solid oxide fuel cells. *J. Mater. Sci.*, 2003, **38**, 507–513.
8. Caplan, D. and Cohen, M., The volatilization of chromium oxide. *J. Electrochem. Soc.*, 1961, **108**, 438–442.
9. Taniguchi, S., Kadowaki, M., Kawamura, H., Yasuo, T., Akiyama, Y., Miyake, Y. *et al.*, Degradation phenomena in the cathode of a solidoxide fuel cell with an alloy separator. *J. Power Sources*, 1995, **55**, 73–79.
10. Jiang, S. P., Zhang, J. P. and Foger, K., Deposition of chromium species at Sr-doped $LaMnO_3$ electrodes in solid oxide fuel cells—II. Effect on O_2 reduction reactions. *J. Electrochem. Soc.*, 2000, **147**, 3195–3205.
11. Jiang, S. P., Zhang, J. P., Apateanu, L. and Foger, K., Deposition of chromium species on Sr-doped $LaMnO_3$ electrodes in solid oxide fuel cells—I. Mechanism and kinetics. *J. Electrochem. Soc.*, 2000, **147**, 4013–4022.
12. Hou, P. Y. and Stringer, J., The effect of reactive element additions on the selective oxidation, growth and adhesion of chromia scales. *Mater. Sci. Eng. A*, 1995, **202**, 1–10.
13. Quadakkers, W. J., Greiner, H., Hänsel, M., Pattanaik, A., Khanna, A. S. and Malléner, W., Compatibility of perovskite contact layers between cathode and metallic interconnector plates of SOFCs. *Solid State Ionics*, 1996, **91**, 55–67.
14. Kim, J.-H., Song, R.-H. and Hyun, S.-H., Effect of slurry-coated $LaSrMnO_3$ on the electrical property of Fe–Cr alloy for metallic interconnect of SOFC. *Solid State Ionics*, 2004, **174**, 185–191.
15. Li, J. Q. and Xiao, P., Fabrication and characterisation of $La_{0.8}Sr_{0.2}MnO_3$/metal interfaces for application in SOFCs. *J. Eur. Ceram. Soc.*, 2001, **21**, 659–668.
16. Fujita, K., Ogasawara, K., Matsuzaki, Y. and Sakurai, T., Prevention of SOFC cathode degradation in contact with Cr-containing alloy. *J. Power Sources*, 2004, **131**, 261–269.
17. Jiang, S. P., Issues on development of (La, Sr)MnO_3 cathode for solid oxide fuel cells. *J. Power Sources*, 2003, **124**, 390–402.
18. Decorse, P., Caboche, G. and Dufour, L.-C., A comparative study of the surface and bulk properties of lanthanum–strontium–manganese oxides $La_{1-x}Sr_xMnO_3$ as a function of Sr-content, oxygen potential and temperature. *Solid State Ionics*, 1999, **117**, 161–169.
19. Jiang, S. P., Love, J. G., Zhang, J. P., Hoang, M., Ramprakash, Y., Hughes, A. E. *et al.*, The electrochemical performance of LSM/zirconia–yttria interface as a function of a-site non-stoichiometry and cathodic current treatment. *Solid State Ionics*, 1999, **121**, 1–10.
20. Jiang, S. P., Zhang, J. P., Ramprakash, Y., Milosevic, D. and Wilshier, K., An investigation of shelf-life of strontium doped $LaMnO_3$ materials. *J. Mater. Sci.*, 2000, **35**, 2735–2741.
21. Minh, N. Q., Ceramic fuel cells. *J. Am. Ceram. Soc.*, 1993, **76**, 563.
22. Cox, M. G. E., McEnanay, B. and Scott, V. D., A chemical diffusion model for partitioning of transition elements in oxide scales on alloys. *Philos. Mag.*, 1972, **26**, 839–851.
23. Kurokawa, H., Kawamura, K. and Maruyama, T., Oxidation behavior of Fe–16Cr alloy interconnect for SOFC under hydrogen potential gradient. *Solid State Ionics*, 2004, **168**, 13–21.
24. *CRC Handbook of Chemistry and Physics (67th ed.)*, 1986, F-60/61.

25. Peck, D.-H., Miller, M. and Hilpert, K., Vaporization and thermodynamics of $La_{1-x}Sr_xCrO_3$ investigated by Knudsen effusion mass spectroscopy. *Solid Oxide Ionics*, 2001, **143**, 401–412.
26. Zhu, J. H., Zhang, Y., Basu, A., Lu, Z. G., Paranthaman, M., Lee, D. F. *et al.*, $LaCrO_3$-based coatings on ferritic stainless steel for solid oxide fuel cell interconnect application. *Surf. Coat. Technol.*, 2004, **177/178**, 65–72.
27. Speidel, D. H. and Muan, A., The system manganes oxides-Cr_2O_3 in air. *J. Am. Ceram. Soc.*, 1963, **46**, 577–578.
28. Jiang, S. P., Zhang, J. P. and Zheng, X. G., A comparative investigation of chromium deposition at air electrodes of solid oxide fuel cells. *J. Eur. Ceram. Soc.*, 2002, **22**, 361–373.
29. Jiang, S. P. and Love, J. G., Origin of the initial polarization behavior of Sr-doped $LaMnO_3$ for O_2 reduction in solid oxide fuel cells. *Solid State Ionics*, 2001, **138**, 183–190.
30. Viitanen, M. M., Welzenis, R. G. V., Brongersma, H. H. and van Berkel, F. P. F., Silica poisoning of oxygen membranes. *Solid State Ionics*, 2002, **150**, 223–228.